Sub-arcsecond Imaging of SiO in the HH 211 Protostellar Jet

Claire J. Chandler

National Radio Astronomy Observatory, PO Box O, Socorro, NM 87801, USA

and

John S. Richer

Mullard Radio Astronomy Observatory, Cavendish Laboratory, Madingley Road, Cambridge CB3 0HE, United Kingdom

cchandle@nrao.edu, jsr@mrao.cam.ac.uk

ABSTRACT

We present images of the HH 211 molecular jet in the SiO v=0, J=1–0 line at 43 GHz made with the Very Large Array at approximately 0.5 arcsec resolution. The SiO emission appears to trace primarily internal bowshocks in the outflow, suggesting that the dust and molecular gas are accelerated via prompt entrainment at internal working surfaces in the jet. There is also some evidence for limb-brightening of the SiO emission, indicating that SiO emission may also arise from entrainment in the jet's boundary layer. Excitation temperatures of $\gtrsim 150$–200 K are inferred from the SiO emission. Enhancements in the SiO abundance of $\sim 10^6$ over interstellar values are observed, and the possible origin of the SiO is discussed.

Subject headings: ISM: jets and outflows — ISM: molecules — radio lines: ISM — stars: formation

1. Introduction

Ever since protostellar outflows were first discovered our understanding of their driving mechanism has been limited by poor spatial resolution. As a consequence, early measurements (e.g., Snell, Loren, & Plambeck 1980; Lada 1985) suggested the flows had relatively small length-to-width ratios, and the first models concentrated on explaining high-velocity molecular gas as being driven by wind-angle protostellar winds (e.g., Barral & Cantó 1981; Königl 1982; Boss 1987; Shu et al. 1991). This ruled out on morphological grounds the possibility that Herbig-Haro (HH) jets, traced by low-excitation optical lines, were responsible for the molecular flows. However, more recent, higher resolution molecular observations made with large single dishes and millimetre-wave interferometers have demonstrated that the molecular flows frequently possess highly-collimated components (e.g., Bachiller & Cernicharo 1990), and that these are often closely associated with HH objects (Richer et al. 1989). A large number of highly-collimated molecular outflows

have now been detected, and it is commonly assumed that these flows, at least in the younger sources, are driven by the momentum of a high Mach number, neutral jet (Richer et al. 2000).

The detailed physics of how neutral jets, with densities comparable to that of the surrounding material, accelerate molecular gas to generate the molecular flow remain unclear, although several models have been proposed. Material can in principle be entrained in the leading bowshock (e.g., Raga & Cabrit 1993), internal bowshocks (e.g., Raga et al. 1993), and in a turbulent mixing layer along the edges of the jet (Stahler 1994; Taylor & Raga 1995). In most cases, however, the angular resolution of current observations is insufficient to resolve the details of these processes. What is needed is a shock tracer similar to the molecular hydrogen lines at 2 μm, but which does not suffer the obscuration prevalent at optical and near-infrared wavelengths.

The SiO molecule is a very useful tool for investigating jet-cloud interactions (e.g., Martín-Pintado, Bachiller, & Fuente 1992). It can be observed at high angular resolution in the millimetre wavebands, and it seems to be excited primarily in shocks where silicon is removed from dust grains, significantly increasing its gas phase abundance. Thermal emission from its vibrational ground state lines has been detected in a number of protostellar outflow sources, and it appears to be intimately associated with collimated jets (e.g., L1448: Guilloteau et al. 1992) rather than with the general, low-velocity outflow traced by CO emission. Models suggest that SiO most likely originates from the sputtering of silicon atoms off silicate grains in C-shocks having speeds in the range 10 to 50 km s^{-1}, followed by rapid conversion to SiO in the gas phase (Field et al. 1997; Schilke et al. 1997; Caselli, Hartquist, & Havnes 1997). Abundance enhancements of 4 to 5 orders of magnitude over the very low gas-phase abundance of SiO in the ambient interstellar medium have been observed in some outflows (e.g., Bachiller, Martín-Pintado, & Fuente 1991; Mikami et al. 1992; Bachiller et al. 1994). The lack of foreground extinction at millimetre wavelengths also make the rotational transitions of SiO particularly important for studies of the youngest outflows, which are associated with the most deeply embedded protostars.

The protostar driving the HH 211 system is one of the youngest and most deeply embedded low-mass protostars known. It was discovered serendipitously through its bright, shocked, H_2 2-μm emission in an imaging study of the IC348 region (McCaughrean, Rayner, & Zinnecker 1994), and lies at a distance of ~ 350 pc (Herbig & Jones 1983). Although given a Herbig-Haro catalogue number, no *optical* emission has yet been detected from this object, most likely due to the high obscuration. The H_2 image shows a compact, well-collimated flow which is also detected in CO emission (Gueth & Guilloteau 1999). Because of the relatively small projected CO flow speeds (< 20 km s^{-1}), and the high degree of separation of the red and blue lobes, the outflow's inclination to the plane of the sky is probably small; if the true CO flow speeds are > 100 km s^{-1} as in other outflows, the implied inclination is less than 10°. Between the two lobes, the driving protostar is detected as a millimetre continuum source with no 2-μm or optical counterpart, designated HH 211-mm by Gueth & Guilloteau (1999). The outflow's age, and hence that of the protostar, can be estimated from the outflow properties, although various assumptions need to be made. The value derived by Gueth & Guilloteau (1999) is only 750 years, suggesting that the embedded protostar has only just entered its main accretion and outflow phase, and making it an ideal object in which to study the early stages of low mass star formation. Here we have taken advantage of the high resolution available with the Very Large Array (VLA) at 43 GHz to study the SiO v=0, J=1–0 emission from the HH 211 protostellar

jet, and to investigate the entrainment and acceleration of molecular outflows.

2. Observations and data reduction

Observations of HH 211 in the v=0, J=1–0 transition of SiO at 43.4 GHz were made using 10 antennas of the VLA of the National Radio Astronomy Observatory[1]. The FWHM of the primary beam of the VLA antennas at this frequency is approximately 1 arcmin. The first observations took place in the compact D configuration, in 1996 August; we re-observed HH 211 using the more extended C configuration in 1997 September to obtain higher resolution images. On each occasion, two circular polarisations were measured each with 16 Hanning-smoothed channels, providing a spectral resolution of 781.25 kHz (5.4 km s^{-1}).

In D configuration two phase centers were observed, one toward the red outflow lobe and one toward the blue. The positions are listed in Table 1. Atmospheric and instrumental phase fluctuations were monitored every 10 minutes by observing the quasar Pks 0333+321, and the pointing was corrected using 8.4 GHz observations of this same quasar at intervals of approximately one hour. The bandpass response was obtained from observations of 3C84. The absolute flux density scale was determined from 3C48, with an assumed 43 GHz flux density of 0.57 Jy, to give a measured 43 GHz flux density for 0333+321 of 1.40 ± 0.03 Jy. The remaining 14 VLA antennas were used to search for 22.2 GHz H_2O maser emission within the primary beam of 2 arcmin (FWHM). A single IF with right circular polarisation was used with 64 Hanning-smoothed channels covering a total bandwidth of 6.25 MHz (84.3 km s^{-1}), centered on $V_{\rm LSR} = 0$ km s^{-1}. A single phase center was observed, and the same quasar was used at 22.2 GHz for the phase, bandpass, and flux density calibration as at 43.4 GHz. The synthesised beam was $3\farcs1 \times 2\farcs5$ at PA = 73°, and the rms noise per channel was 9 mJy per beam. No H_2O emission was detected from HH 211.

The C-array observations used a single phase center, at the location of the protostar. The atmospheric phase fluctuations on the longer baselines in C configuration are significantly worse than in D, so we used a much faster switching time between the source and 0333+321, with a total cycle time from source to calibrator to source of 1 min 40 sec. The pointing was checked every hour using 8.4 GHz observations of 0333+321, and the bandpass was obtained from 3C84. The absolute flux density scale was determined from 3C286, with an assumed 43 GHz flux density of 1.45 Jy, to give a 43 GHz flux density for 0333+321 of 2.08 ± 0.08 Jy on this occasion. The uncertainty in the absolute flux density scale for both datasets is approximately 15%.

The data were calibrated, imaged, and CLEANed using the AIPS reduction package, and the synthesised beam, which is intermediate between uniform and natural weighting ("robust" weighting: Briggs 1995), is optimised for a combination of resolution and sensitivity. The CLEAN beam widths and rms noise per channel at the center of each field are listed in Table 1; however, because the two fields in D configuration were corrected for the response of the primary beam and coadded, they have both been restored with the

[1]The National Radio Astronomy Observatory is a facility of the National Science Foundation operated under cooperative agreement by Associated Universities, Inc.

average synthesised beam listed in column 5. All the quantitative results described below are derived from CLEANed images of the data obtained in each VLA configuration separately. However, images have also been made by combining the C and D-array data and carrying out a joint deconvolution of the synthesized beams using the maximum entropy routine UTESS in AIPS. These images are displayed in Figs 1 and 2, but because the resolution is a function of the local signal-to-noise ratio after maximum-entropy processing, the UTESS images have not been used in any of the quantitative analyses.

3. Results and discussion

3.1. Structure and kinematics

Fig. 1 shows the integrated red and blueshifted SiO(1–0) emission from HH 211 overlaid on a logarithmic greyscale image of the shocked molecular hydrogen emission from McCaughrean et al. (1994). The SiO is mainly located inside the outer faint shell of H_2 emission, is well collimated, and appears to be associated only with the jet from the exciting star. It corresponds closely to the strongest emission peaks in the high-velocity CO(2–1) map of Gueth & Guilloteau (1999). While the SiO emission on the jet axis is generally coincident with regions of shocked H_2 (in the case of the redshifted component, even terminating at an H_2 knot), no emission is detected at the brightest H_2 peaks despite the fact that they fall well inside the 50% response level of the VLA D-array observations (dashed contour, Fig. 1). This lack of detailed correlation between the two shock tracers is also seen in other young outflows (e.g., IRAS 03828+3035: Bachiller et al. 1994; L1157: Gueth, Guilloteau, & Bachiller 1998), and possible explanations are discussed further in § 3.2 below.

Between the position of the protostar and a projected angular distance of $15''$ both the red and blue components of the SiO jet gradually widen. Little or no redshifted SiO is detected beyond $15''$, although knots and other features continue out to larger distances on the blueshifted side. The total flux in the blueshifted and redshifted SiO jets of HH 211 is comparable, but Fig. 1 shows that the blue emission is more diffuse than the red, a feature which is illustrated quite dramatically in maps of the emission made within individual velocity channels (Fig. 2). The systemic velocity, $V_{\rm sys}$, of the molecular cloud is at $V_{\rm LSR} \sim 9$ km s^{-1} (Gueth & Guilloteau 1999), and at a radial velocity $|V - V_{\rm sys}| \sim 10$ km s^{-1} the full width zero intensity of the blueshifted emission is $\sim 4''$, twice that on the redshifted side. A further difference between the structures of the red and blue SiO jets is in their association with infrared H_2 emission: the one strong peak in the blueshifted jet, at $V_{\rm LSR} = -0.8$ km s^{-1}, corresponds closely to a bright H_2 knot, while the redshifted SiO is coincident only with very faint H_2 emission. These features are most easily explained by the structure of the molecular cloud core in which HH 211 resides. The core exhibits a steep density gradient in the direction of the blueshifted side of the jet, compared with the considerable amounts of dense gas on the redshifted side (traced by $H^{13}CO^+$(1–0) emission: see Gueth & Guilloteau 1999) into which the redshifted jet must penetrate. The decreased pressure of the ambient gas on the blueshifted side may allow the jet to expand more freely perpendicular to the jet direction. Toward the redshifted SiO jet the dense gas results in high foreground extinction for the infrared H_2 emission.

In three of the redshifted channels, from $V_{\rm LSR}$ = 20.8 to 31.6 km s^{-1}, the SiO emission divides into two streamers separated by $\sim 1''$, and appears to be the limb-brightening of a layer of molecular material around the faint H_2 jet. At several locations the bifurcated streamers seem to lie behind (i.e., closer to the protostar) a knot of SiO emission on the jet axis that is at a higher velocity. Such a configuration suggests that the SiO is accelerated at internal bowshocks within the jet, and, indeed, may be formed in these bowshocks. Alternatively, the limb brightening may be the result of laminar entrainment of SiO along the edges of the jet.

The kinematics of the SiO jet matches closely that of the high-velocity CO(2–1) detected by Gueth & Guilloteau (1999). The SiO emission in the images made from only C-array data is very clumpy, and may be missing flux particularly in the blueshifted channels. We therefore use only emission detected at a level of 3σ or greater in the VLA D configuration in analyzing the overall velocity structure of the SiO jet. Fig. 3a shows the first moment (intensity-weighted mean velocity) of the SiO(1–0), overlaid with contours of shocked H_2 emission. It illustrates that the ends of the jets are the locations of highest radial velocity compared to the ambient cloud. An approximately uniform velocity gradient along the jet (sometimes called a "Hubble-law flow") can also be seen, and the value of the gradient, $\sim 5 \times 10^{-3}$ km s^{-1} AU^{-1}, is very similar to that measured from the CO(2–1) emission. The redshifted lobe in particular shows a smooth velocity gradient along the jet, with a maximum at 30 km s^{-1} away from $V_{\rm sys}$. The second moment map of the SiO emission (Fig. 3b) shows that the positions of highest velocity dispersion generally coincide with the brightest shocked H_2 emission on the jet axis, providing further evidence that the SiO is in some way associated with, or possibly formed in, those jet shocks.

3.2. Excitation, abundance, and origin of the SiO

The peak beam-averaged brightness temperature, $T_{\rm B}$, in the C-array data is 54 K, and occurs in the channel at $V_{\rm LSR} = 26.2$ km s^{-1}, providing a firm lower limit on the excitation temperature, $T_{\rm ex}$, within the redshifted gas. In the blueshifted lobe the peak at $V_{\rm LSR} = -0.8$ km s^{-1} corresponds to $T_{\rm B} = 47$ K. Further constraints on $T_{\rm ex}$ can be obtained by comparing the J=1–0 line with spectra of the SiO(5–4) emission obtained with the James Clerk Maxwell Telescope in a $22''$ beam (Chandler & Richer 1997; Fig. 4). The integrated J=1–0 flux from the C and D-array VLA images are the same to within the calibration uncertainties, and the SiO jet is unresolved laterally in the images made from data obtained only in the VLA D configuration. We therefore assume that the D-array observations did not resolve out any of the 1–0 emission. If all the SiO is at the same temperature and in local thermodynamic equilibrium both the SiO(5–4)/(1–0) line ratio and the peak $T_{\rm B}$ can therefore be combined to give the line optical depths and a lower limit to $T_{\rm ex}$. We find for the red jet that the J=1–0 optical depth, τ_{10}, is ~ 0.28, and $T_{\rm ex} \gtrsim 220$ K, while for the blue jet $\tau_{10} \sim 0.36$ and $T_{\rm ex} \gtrsim 155$ K. These limits do not include uncertainties in the flux calibration of the J=1–0 and 5–4 spectra, and assuming a 15% uncertainty in both gives strict lower limits to $T_{\rm ex}$ of 185 K (red) and 120 K (blue). Such temperatures are considerably higher than the ~ 10 K expected for the ambient molecular gas and dust. Very high space densities in the emitting gas are also implied by the detection of the SiO(5–4) line, which has a critical density of order 10^6 cm^{-3}. These results confirm that

the SiO originates in regions of extreme excitation conditions.

The total mass of the high-velocity CO jet determined assuming a CO abundance of 10^{-4} is $\sim 2.5 \times 10^{-3} (T_{\rm ex}/50\ {\rm K})\ {\rm M}_\odot$ (Gueth & Guilloteau 1999). Assuming the SiO and high-velocity CO(2–1) emission are co-spatial (but do not necessarily have the same excitation temperature) a value $T_{\rm ex} = 150$ K for the SiO gives an SiO abundance $X({\rm SiO}) \sim 6 \times 10^{-6}$, comparable to that determined for the high-velocity gas in the L1448 jet by Martín-Pintado et al. (1992), who derive $X({\rm SiO}) \sim 2 \times 10^{-6}$. In HH 211, however, the SiO emission is not as extended as the high-velocity CO jet, and so our value for X(SiO) is likely to be a lower limit. The abundance of SiO is therefore enhanced by approximately a factor of 10^6 over that typically observed in quiescent molecular clouds, where $X({\rm SiO}) \lesssim 10^{-11}$ (Ziurys, Friberg, & Irvine 1989). Such a high abundance suggests that at least 10% of all the silicon is in the form of SiO, requiring an extremely efficient mechanism for releasing Si from dust grains into the gas phase, to enable subsequent gas-phase chemistry to produce SiO.

Two mechanisms have been proposed for increasing the amount of gas-phase silicon in shocks. In J-shocks and slow C-shocks grain-grain collisions may be the dominant means of destroying the grains to release refractory elements (Seab & Shull 1983; Jones et al. 1994; Caselli et al. 1997), while in faster C-shocks the sputtering of grain mantles and refractory cores by heavy ions is a more efficient process (Field et al. 1997; Schilke et al. 1997; Caselli et al. 1997). Once produced the SiO may be destroyed in shocks by reactions such as SiO + C $\rightarrow$ CO + Si, SiO + OH $\rightarrow$ SiO_2 + H, and SiO + $h\nu$ $\rightarrow$ SiO^+ + e (e.g., Hartquist, Oppenheimer, & Dalgarno 1980; Neufeld & Dalgarno 1989). It may also be depleted back onto dust grains in the post-shock gas.

Both the extremely localized nature of the SiO emission from the HH 211 jet, and the plausible explanations for producing the observed large abundance enhancements via the destruction of dust grains in shocks, suggest that dust must be located either within the jet itself, or in a cocoon of material surrounding the jet and from which the jet can entrain the dust. However, the separation of the CO(2–1) into two distinct kinematic components by Gueth & Guilloteau (1999) — a low-velocity shell and a high-velocity, highly-collimated jet, with no evidence for molecular material at intermediate velocities or in the cavity between the shell and the jet — makes it seem most likely that the dust originates at the base of the jet, from where the dust is entrained or injected directly into the jet. If the limb-brightened edges of the SiO jet are indicative of lateral entrainment the dust must either be destroyed locally in shocks long the edges of the jet, or the SiO must already be formed at the jet base.

The observed location and velocity of the SiO emission are consistent with its production in C-shocks, with speeds in the range 10–50 km s^{-1}. Such shock conditions are also believed to produce most of the observed H_2 emission from outflow sources (e.g., Smith, Brand, & Moorhouse 1991), which would lead us to expect a much better correlation between SiO and H_2 emission than is observed. Although the SiO peaks in Fig. 1 do lie on areas of strong H_2 emission, beyond the SiO jet, at distances greater than $20''$ (7000 AU) from the driving source, the H_2 remains strong while there is no detectable SiO emission. A lack of precise correspondence between SiO and H_2 emission is also observed in IRAS 03282+3035 and L1157, but for these sources the SiO emission tends to lie downstream from strong H_2 emission, and each

tracer is assumed to be following different physical and chemical conditions in the evolution of the post-shock gas (Bachiller et al. 1994; Gueth et al. 1998). One possible explanation for the lack of detectable SiO emission near the brightest H_2 peaks in HH 211 is that although gas-phase SiO is being produced in the shocks, the post-shock density is insufficient to collisionally excite the rotational lines; such a picture is consistent with the SiO primarily being produced close to the driving source, where the envelope densities are highest. Alternatively, it is possible that one of the two SiO destruction processes referred to above is operating efficiently in the shocks occurring further from the driving protostar.

4. Conclusions

The SiO images of the HH 211 jet presented in this paper are among the highest resolution images of a protostellar jet: the resolution of $0.5''$ corresponds to only 170 AU, and is sufficient to resolve the width of the jet as traced by SiO emission. The SiO emission is extremely clumpy, and arises in multiple compact knots whose scale is much smaller than the coherent shocked structures traced by H_2 emission. The most likely origin for these SiO structures is in internal bowshocks generated by a time-dependent jet velocity. The clumpy nature of the SiO emission suggests these shocks have a very complex spatial structure, most likely due to Raleigh-Taylor instabilities in the cooling, post-shock gas. There is also some morphological evidence for limb-brightened SiO emission, which could arise in a hot boundary layer between the jet and the surrounding material, but this pattern of emission could equally well be generated in the tails of an internal bowshock. Although the SiO detected does coincide with the strong H_2 peaks close to the driving protostar, no SiO emission is detected at projected distances of more than $20''$, despite these being the locations of the strongest H_2 knots. This result suggests that the shock conditions, perhaps the pre-shock density, vary rapidly along the length of the jet.

Acknowledgments

The authors are very grateful to Mark McCaughrean for providing the image of shocked molecular hydrogen emission associated with HH 211, and thank the referee for making useful comments that have helped clarify the paper. CJC was supported by a PPARC Advanced Fellowship during part of this work, and JSR is partially supported by a Royal Society Fellowship.

REFERENCES

Bachiller, R., & Cernicharo, J. 1990, A&A, 239, 276

Bachiller, R., Martín-Pintado, J., & Fuente, A. 1991, A&A, 243, L21

Bachiller, R., Terebey, S., Jarrett, T., Martín-Pintado, J., Beichman, C. A., & Van Buren, D. 1994, ApJ, 437, 296

Barral, J. F., & Cantó, J. 1981, Rev. Mex. Astr. Ap., 5, 101

Boss, A. P. 1987, ApJ, 316, 721

Briggs, D. S. 1995, PhD Thesis, New Mexico Institute of Mining and Technology

Caselli, P., Hartquist, T. W., & Havnes, O. 1997, A&A, 322, 296

Chandler, C. J., & Richer, J. S. 1997, in Low Mass Star Formation – from Infall to Outflow: Poster proceedings of IAU Symposium No. 182 on Herbig-Haro Objects and the Birth of Low Mass Stars, eds F. Malbet & A. Castets, 76

Field, D., May, P. W., Pineau des Forêts, G., & Flower, D. R. 1997, MNRAS, 285, 839

Gueth, F., Guilloteau, S., & Bachiller, R. 1998, A&A, 333, 287

Gueth, F., & Guilloteau, S. 1999, A&A, 343, 571

Guilloteau, S., Bachiller, R., Fuente, A., & Lucas, R. 1992, A&A, 265, L49

Hartquist, T. W., Oppenheimer, M., & Dalgarno, A. 1980, ApJ, 236, 182

Herbig, G. H., & Jones, B. F. 1983, AJ, 88, 1040

Jones, A. P., Tielens, A. G. G. M., Hollenbach, D. J., & McKee, C. F. 1994, ApJ, 433, 797

Königl, A. 1982, ApJ, 261, 115

Lada, C. J. 1985, ARA&A, 23, 267

Martín-Pintado, J., Bachiller, R., & Fuente, A. 1992, A&A, 254, 315

McCaughrean, M. J., Rayner, J. T., & Zinnecker, H. 1994, ApJ, 436, L189

Mikami, H., Umemoto, T., Yamamoto, S., & Saito, S. 1992, ApJ, 392, L87

Neufeld, D. A., & Dalgarno, A. 1989, ApJ, 340, 869

Raga, A., & Cabrit, S. 1993, A&A, 278, 267

Raga, A. C., Cantó, J., Calvet, N., Rodríguez, L. F., & Torrelles, J. M. 1993, A&A, 276, 539

Richer, J. S., Hills, R. E., Padman, R., & Russell, A. P. G. 1989, MNRAS, 241, 231

Richer, J. S., Shepherd, D. S., Cabrit, S., Bachiller, R., & Churchwell, E. 2000, in Protostars and Planets IV, eds V. Mannings, A. P. Boss, & S. S. Russell (Tucson: University of Arizona Press), 867

Schilke, P., Walmsley, C. M., Pineau des Forêts, G., & Flower, D. R. 1997, A&A, 321, 293

Seab, C. G., & Shull, J. M. 1983, ApJ, 275, 652

Shu, F. H., Ruden, S. P., Lada, C. J., & Lizano, S. 1991, ApJ, 370, L31

Smith, M. D., Brand, P. W. J. L., & Moorhouse, A. 1991, MNRAS, 248, 451

Snell, R. L., Loren, R., & Plambeck, R. L. 1980, ApJ, 239, L17

Stahler, S. W. 1994, ApJ, 422, 616

Taylor, S. D., & Raga, A. C. 1995, A&A, 296, 823

Ziurys, L. M., Friberg, P., & Irvine, W. M. 1989, ApJ, 343, 201

This preprint was prepared with the AAS LaTeX macros v5.0.

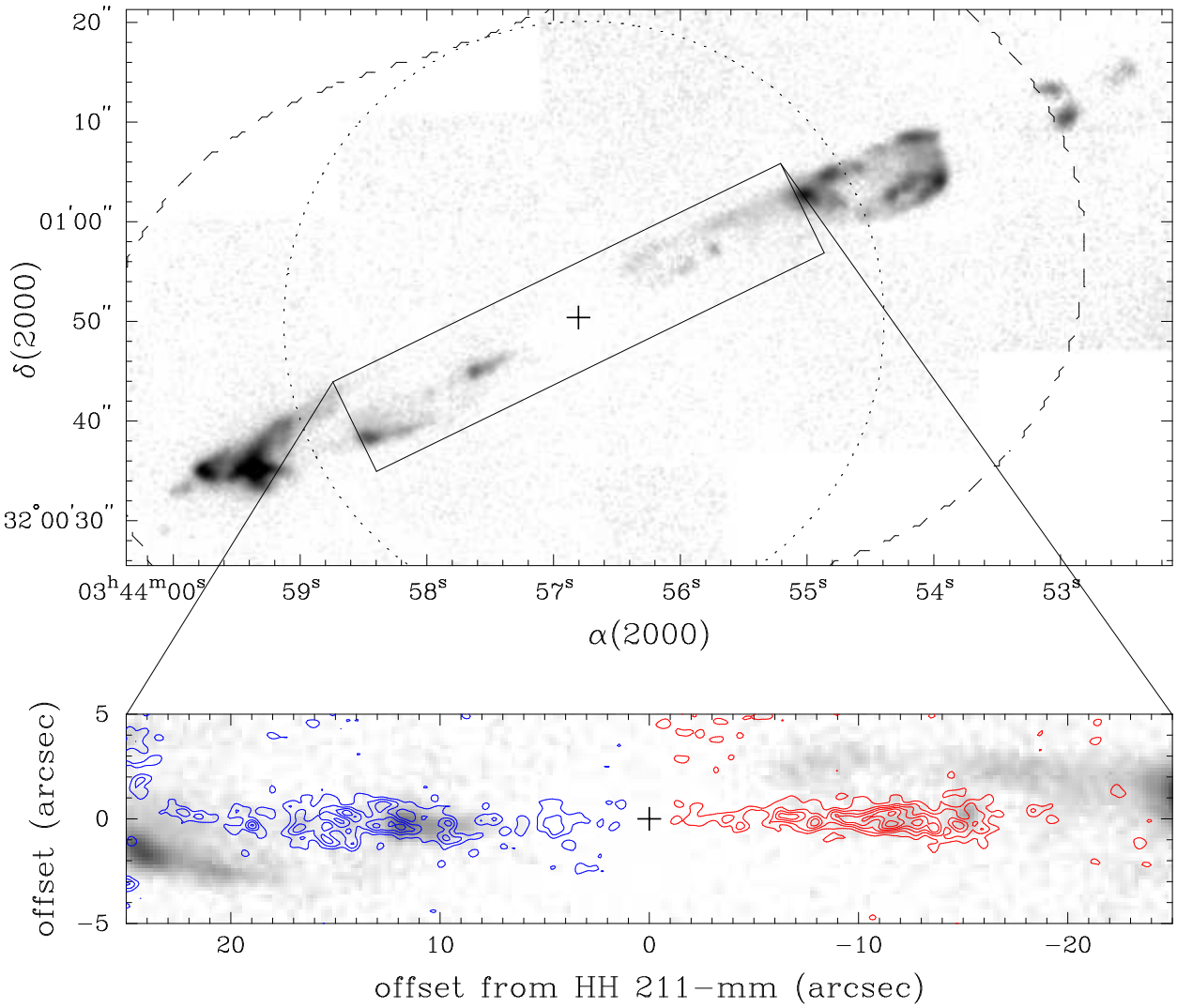

Fig. 1.— *Top:* Logarithmic greyscale image of the near-infrared H_2 emission from HH 211, from McCaughrean et al. (1994). The dashed contour outlines the 50% sensitivity level of the VLA observations obtained in D configuration, and the dotted contour describes the same for the C-array data. The cross marks the position of the protostar, HH 211-mm, from Gueth & Guilloteau (1999). No SiO (1–0) emission was detected in C or D configuration outside the box (solid contour) centered on the protostar. *Bottom:* Expanded image of the box centered on HH 211-mm, rotated by $-26°$ to align it with the horizontal. The infrared H_2 is in greyscale, and is overlaid by the integrated blueshifted (blue contours, to the east of the protostar) and redshifted (red contours, to the west) SiO(1–0) emission imaged with the VLA. Contours begin at, and are spaced at intervals of, 3 mJy arcsec^{-2}.

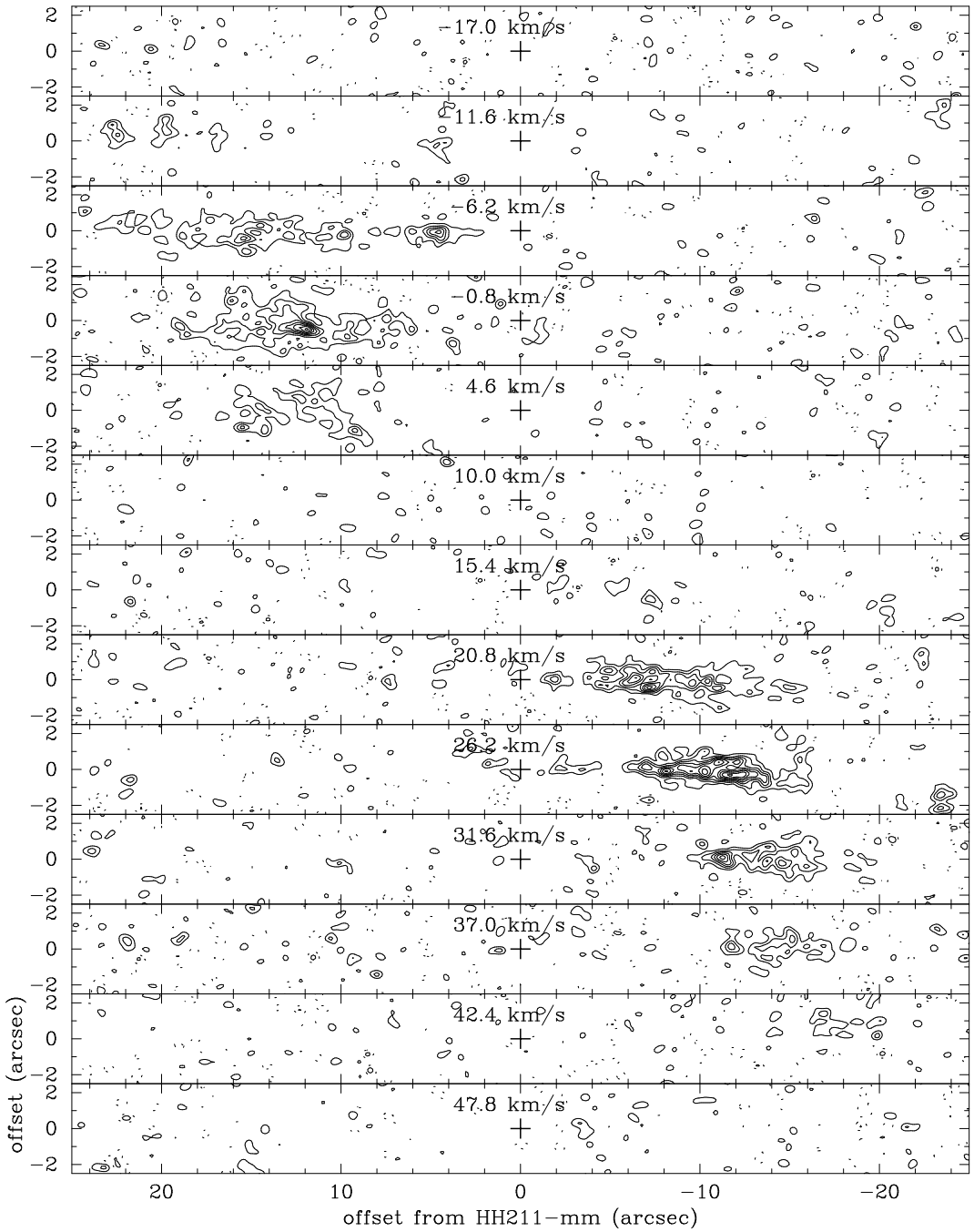

Fig. 2.— Channel maps of the SiO(1–0) emission from HH 211. The LSR velocity is given at the top of each panel, and contours equally spaced at intervals of 5.2 mJy arcsec^{-2}.

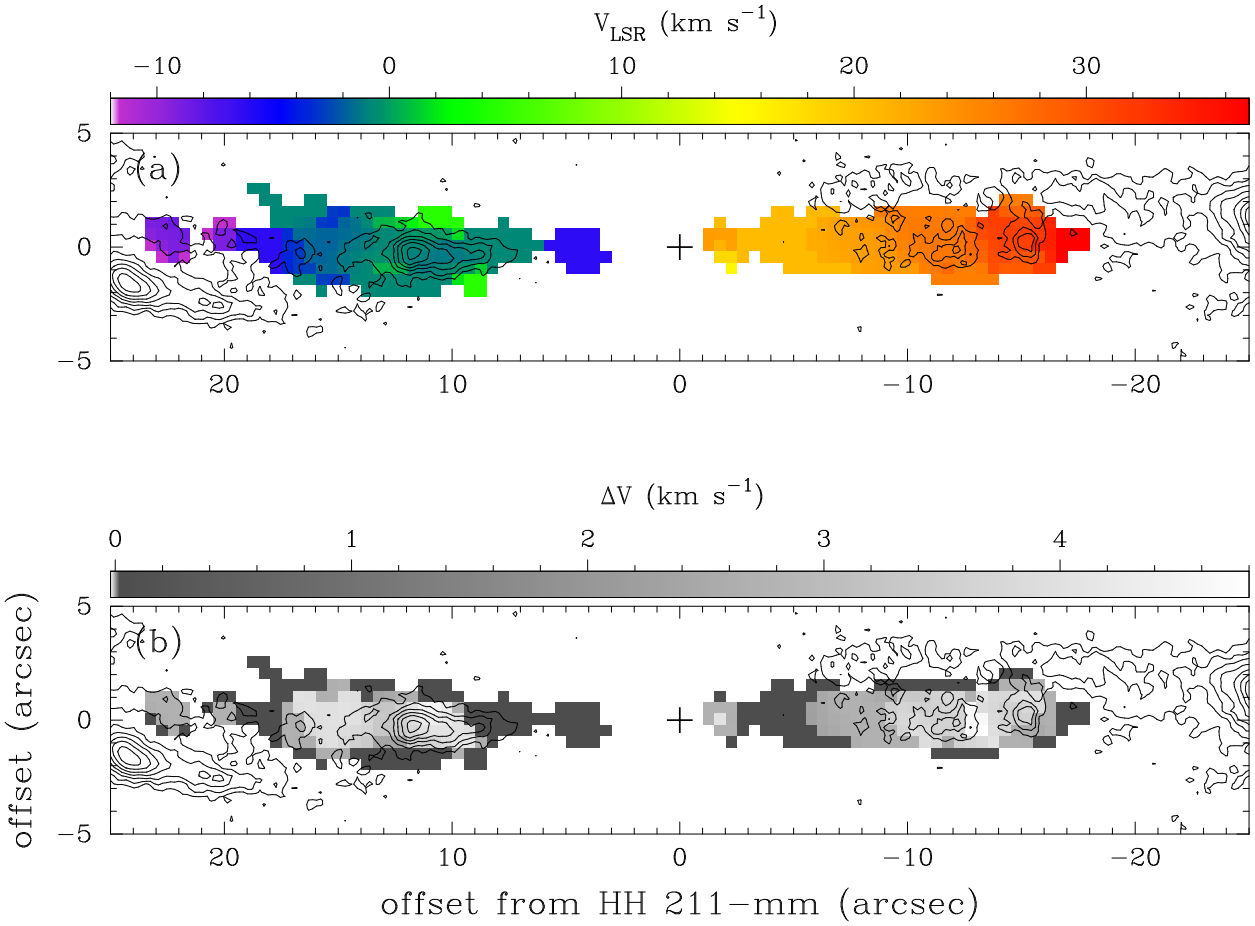

Fig. 3.— (a) The first moment of the SiO(1–0) emission, obtained from the VLA D-array data only, overlaid by contours of the infrared H_2 emission. The color scale runs from $V_{\rm LSR} = -12$ km s^{-1} (blue) to +37 km s^{-1} (red); (b) the second moment of the SiO(1–0) emission, running from $\Delta V = 0$ km s^{-1} to 4.8 km s^{-1}. The highest velocity dispersion of the SiO(1–0) line generally coincides with shocked H_2 emission.

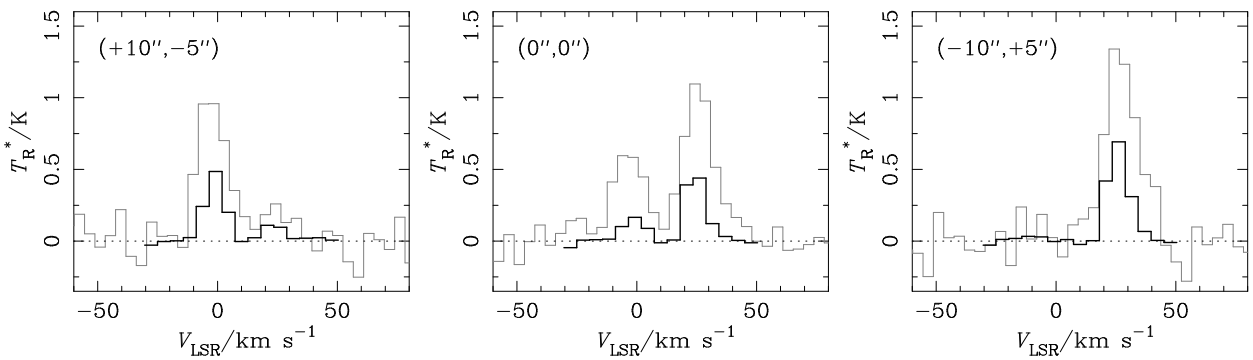

Fig. 4.— Spectra of the SiO(5–4) in grey and SiO(1–0) in black towards the blueshifted jet (left), the protostar (center), and the redshifted jet (right).

Table 1. Summary of the VLA observations of SiO(1–0) in HH 211.

Array	Phase center $\alpha(2000)$ ($^{\rm h}$ $^{\rm m}$ $^{\rm s}$)	Phase center $\delta(2000)$ ($^\circ$ $'$ $''$)	Synthesised beam ($''$)	Restoring beam ($''$)	Rms (mJy beam^{-1})	K mJy^{-1}
D	03 43 58.200	32 00 43.00	2.17×1.43 @ 69°	2.17×1.43 @ 69°	4.5	0.21
	03 43 55.200	32 00 57.00	2.16×1.43 @ 68°	2.17×1.43 @ 69°	4.5	0.21
C	03 43 56.760	32 00 50.00	0.58×0.43 @ −44°	0.58×0.43 @ −44°	2.3	2.6